# Numerical study of flow around flat plate using higher-order accuracy scheme

*Murodil* Madaliev*, *Elmurad* Yunusaliev, *Akramjon* Usmanov, *Nodirakhon* Usmonova, *Khusanboy* Muxammadyoqubov

Fergana Polytechnic Institute, Fergana, 150107, Uzbekistan

**Abstract.** Analytical methods exist to solve the problems of hydromechanics and heat transfer, but it is not possible to obtain the solution to some inhomogeneous and nonlinear problems of hydromechanics and heat transfer by analytical methods. The solution to such problems is carried out using numerical methods. Currently, there are many textbooks and monographs on numerical methods for solving problems of hydromechanics, thermal conductivity, heat and mass transfer, and others. The article presents the results of a numerical study of the flow structure in the flow around a flat plate. The calculations are based on the numerical solution of a system of nonstationary equations using a two-fluid turbulence model. For the numerical solution of these problems, schemes of the second and fourth order of accuracy were applied. The control volume method was used for the difference approximation of the initial equations, and the relationship between velocities and pressure was found using the SIMPLE procedure. To confirm the correctness of the numerical results, comparisons were made with each other and experimental data.

## 1 Introduction

In recent decades, significant progress has been made in developing high-precision numerical methods for solving the Navier-Stokes equations for modeling turbulent flows of practical interest. Computational methods such as large LES vortices modeling and direct numerical DNS modeling are increasingly being applied to such flows. However, their use is still limited by grid resolution requirements and, therefore, by available computational resources. Therefore, their wide practical application is associated with the development of computer technology and, according to experts, can begin only at the end of this century. Therefore, shortly, semi-empirical methods will remain the main working tool for solving applied aerodynamics problems. Most semi-empirical turbulence models are based on the so-called RANS equation. With this approach, in the equations of hydrodynamics, after averaging over time, Reynolds stresses arise, which must be determined. Consequently, the resulting system of equations is obtained unclosed. Many different mathematical models have been proposed to close the resulting system of equations. These models are based on the hypotheses of Boussinesq [1], Prandtl [2], Karman [3], etc. The NASA turbulence database provides a comparative analysis of various semi-empirical models. From this

* Corresponding author: Madaliev.ME2019@mail.ru

analysis, it can be concluded that the most accurate is the Spalart and Allmaras models [4] and the Menter model k-ω SST [5-7]. To date, numerical solutions to many important practical problems have been obtained using these models.

Recently, the two-fluid turbulence model has become increasingly popular [8]. This model is based on the dynamics of two fluids, which, unlike the Reynolds approach, leads to a closed system of equations. This model's peculiarity is that it can describe complex anisotropic turbulent flows. The problem under consideration is of great importance for aviation and rocket-space technology. In [9], a new two-fluid model was used to study the flow past a flat plate. In this case, a simplified, parabolize system of equations was used, i.e., the pressure was assumed to be constant. However, not in all streamlined flows the pressure can be considered constant. For example, the flow can occur in many technical devices in limited spaces. Therefore, in this work, there are two main goals, the first is to test the two-fluid model for the flow around a flat plate using the full system of turbulence equations, the second-first for the turbulence equation, the finite difference schemes of the second and fourth order of Runge-Kutta accuracy were used, and the results were compared with experimental data. This problem is described in the NASA database [10].

### 1.1 Physical and mathematical statements of the problem

A two-dimensional turbulent flow in a flat channel is considered. The physical picture of the analyzed flow and the configuration of the computational domain are shown in Fig. 1.

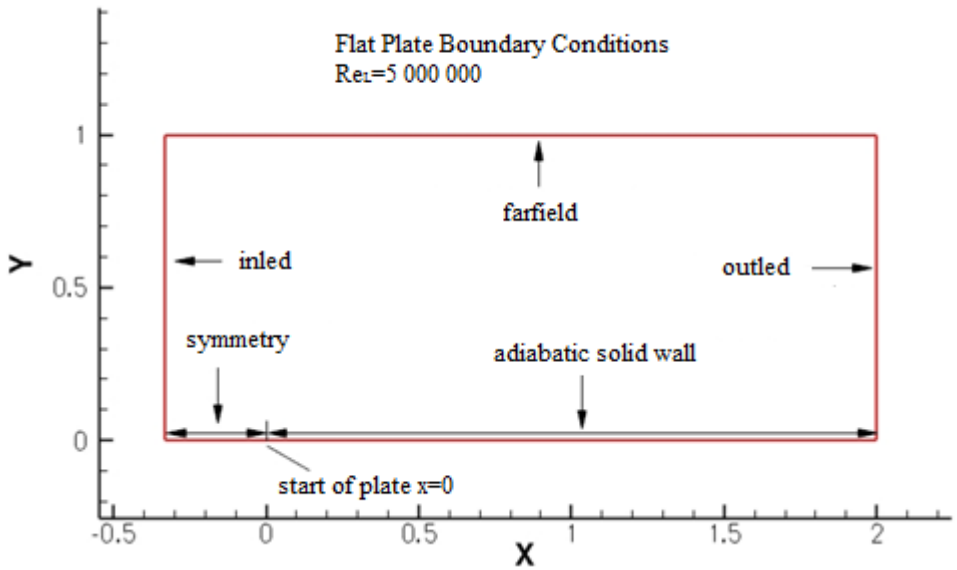


**Fig. 1.** Diagram of the computational domain in a flat channel

The unsteady system of equations of a turbulent two-fluid model in Cartesian coordinates has the following form [11]:

$$
\begin{cases}
\dfrac{\partial \rho}{\partial t}+\dfrac{\partial \rho V_x}{\partial x}+\dfrac{\partial \rho V_y}{\partial y}=0. \\
\dfrac{\partial \rho V_x}{\partial t}+\dfrac{\partial \rho V_x V_x}{\partial x}+\dfrac{\partial \rho V_y V_x}{\partial y}+\dfrac{\partial p}{\partial x}=2\dfrac{\partial}{\partial x}\left(\nu\rho\dfrac{\partial V_x}{\partial x}\right)+\dfrac{\partial}{\partial y}\left(\nu\rho\left(\dfrac{\partial V_x}{\partial y}+\dfrac{\partial V_y}{\partial x}\right)\right)-\dfrac{\partial \rho \vartheta_x \vartheta_x}{\partial x}-\dfrac{\partial \rho \vartheta_x \vartheta_y}{\partial y}; \\
\dfrac{\partial \rho V_y}{\partial t}+\dfrac{\partial \rho V_x V_y}{\partial x}+\dfrac{\partial \rho V_y V_y}{\partial y}+\dfrac{\partial p}{\partial y}=\dfrac{\partial}{\partial x}\left(\nu\rho\left(\dfrac{\partial V_y}{\partial x}+\dfrac{\partial V_x}{\partial y}\right)\right)+2\dfrac{\partial}{\partial y}\left(\nu\rho\dfrac{\partial V_y}{\partial y}\right)-\dfrac{\partial \rho \vartheta_x \vartheta_y}{\partial x}-\dfrac{\partial \rho \vartheta_y \vartheta_y}{\partial y}; \\
\dfrac{\partial \rho \vartheta_x}{\partial t}+\dfrac{\partial \rho V_x \vartheta_x}{\partial x}+\dfrac{\partial \rho V_y \vartheta_x}{\partial y}=-\left(u\rho\dfrac{\partial V_x}{\partial x}+\vartheta\rho\dfrac{\partial V_x}{\partial y}\right)+C_s\rho\left(-\left(\dfrac{\partial V_y}{\partial x}-\dfrac{\partial V_x}{\partial y}\right)\vartheta_y\right)+ \\
+\dfrac{\partial}{\partial x}\left(2\rho\nu_{xx}\dfrac{\partial \vartheta_x}{\partial x}\right)+\dfrac{\partial}{\partial y}\left(\rho\nu_{xy}\left(\dfrac{\partial \vartheta_x}{\partial y}+\dfrac{\partial \vartheta_y}{\partial x}\right)\right)-C_r\rho\vartheta_x; \\
\dfrac{\partial \rho \vartheta_y}{\partial t}+\dfrac{\partial \rho V_x \vartheta_y}{\partial x}+\dfrac{\partial \rho V_y \vartheta_y}{\partial y}=-\left(\vartheta_x\rho\dfrac{\partial V_y}{\partial x}+\vartheta_y\rho\dfrac{\partial V_y}{\partial y}\right)+ \\
+C_s\rho\left(\left(\dfrac{\partial V_y}{\partial x}-\dfrac{\partial V_x}{\partial y}\right)\vartheta_x\right)+\dfrac{\partial}{\partial x}\left(\rho\nu_{xy}\left(\dfrac{\partial \vartheta_y}{\partial x}+\dfrac{\partial \vartheta_x}{\partial y}\right)\right)+\dfrac{\partial}{\partial y}\left(2\rho\nu_{yy}\dfrac{\partial \vartheta_y}{\partial y}\right)-C_r\rho\vartheta_y;
\end{cases}
\quad (1)
$$

Here

$$
\nu_{xx}=\nu_{yy}=\frac{3}{\mathrm{Re}}+2\frac{S}{|\mathbf{defV}|},\ \nu_{xy}=\frac{3}{\mathrm{Re}}+2\left|\frac{\vartheta_x\vartheta_y}{\mathbf{defV}}\right|,\ S=\frac{\vartheta_x{}^2 J_x+\vartheta_y{}^2 J_y}{J_x+J_y},\ J_x=\left|\frac{\partial \vartheta_x}{\partial x}\right|,\ J_y=\left|\frac{\partial \vartheta_y}{\partial y}\right|,
$$

$$
|\mathbf{defV}|=\mu\sqrt{2\left(\left(\frac{\partial V_x}{\partial x}\right)^2+\left(\frac{\partial V_y}{\partial y}\right)^2\right)+\left(\frac{\partial V_y}{\partial x}+\frac{\partial V_x}{\partial y}\right)^2}\ C_s=0.2,\ C_r=C_1\lambda_{\max}+C_2\frac{|\mathbf{d}\cdot\mathbf{v}|}{d^2}
$$

In the above equations, $V_x, V_y$ are the axial and transverse components of the averaged flow velocity vector, respectively, p is the hydrostatic pressure, $\vartheta_x, \vartheta_y$ are the relative axial and transverse components of the fluid velocity, $\nu_{xx}, \nu_{yy}, \nu_{xy}$ are the molecular kinematic viscosity, $\nu$ is the effective molar viscosities, d is the nearest distance to the solid wall, $\lambda_{\max}$ is the largest root of the characteristic equation. The constant coefficients are equal to

$$
C_1=0.7825,\ C_2=0.306,\quad C_s=0.2.
$$

### 1.2 Calculated grids

In this study, the thickening of the mesh near the wall of the plates and the vertical position of the beginning of the plate were used. The calculated grid is shown in Fig. 2.

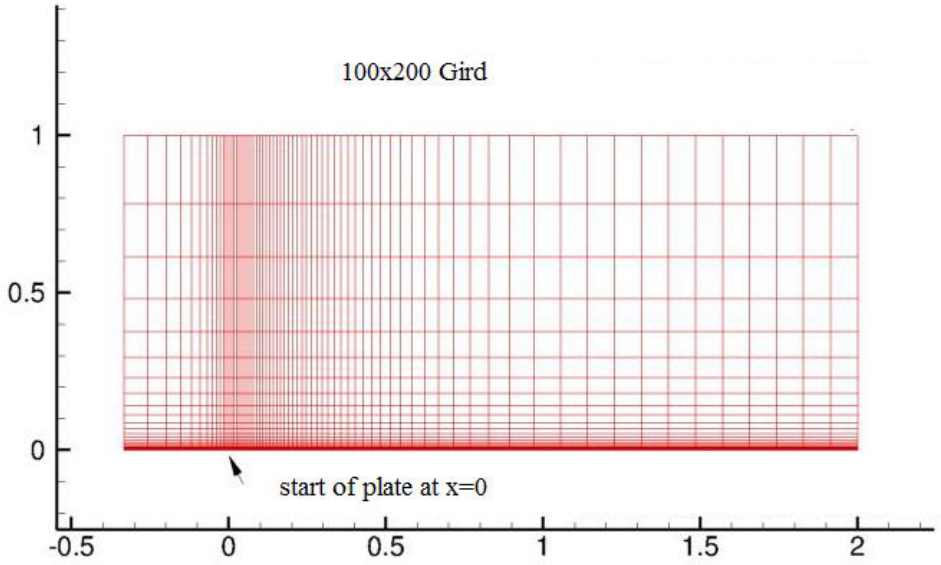


**Fig. 2.** Calculated condensed mesh size 100x200

For this purpose, the transformation of coordinate systems [12] $(x,y)\to(\xi,\eta)$ was used when $x=0$.

$$\xi = x_c\left\{1+\frac{\mathrm{sh}\left[\tau\left(x-B\right)\right]}{\mathrm{sh}\left(\tau B\right)}\right\}, \tag{2}$$

Here

$$B=\frac{1}{2\tau}\ln\left[\frac{1+\left(e^{\tau}-1\right)\left(x_c/L\right)}{1+\left(e^{-\tau}-1\right)\left(x_c/L\right)}\right],\ 0<\tau<\infty,\ x_c=0.333,\ L=2.333. \tag{3}$$

$$\eta=1-\frac{\ln\left(\left\{\beta+1-y/h\right\}/\left\{\beta-1+y/h\right\}\right)}{\ln\left[\left(\beta+1\right)/\left(\beta-1\right)\right]},\quad 1<\beta<\infty,\ h=1. \tag{4}$$

The $\beta$ parameter is about 1 and regulates the degree of grinding. The value $\beta=1.0005,\ \tau=8$ is used in work.

The system of equations (1) after the transformation of coordinates in dimensionless parameters has the following form

$$
\begin{cases}
\dfrac{\partial V_x}{\partial t}+\dfrac{\partial \xi}{\partial x}\dfrac{\partial V_x V_x}{\partial \xi}+\dfrac{\partial \eta}{\partial y}\dfrac{\partial V_y V_x}{\partial \eta}+\dfrac{\partial \xi}{\partial x}\dfrac{\partial p}{\partial \xi}=\dfrac{1}{\mathrm{Re}}\left(\left(\dfrac{\partial \xi}{\partial x}\right)^2\dfrac{\partial V_x}{\partial \xi^2}+\left(\dfrac{\partial \eta}{\partial y}\right)^2\dfrac{\partial^2 V_x}{\partial \eta^2}\right)-\dfrac{\partial \xi}{\partial x}\dfrac{\partial \vartheta_x \vartheta_x}{\partial \xi}-\dfrac{\partial \eta}{\partial y}\dfrac{\partial \vartheta_y \vartheta_x}{\partial \eta};\\
\dfrac{\partial V_y}{\partial t}+\dfrac{\partial \xi}{\partial x}\dfrac{\partial V_x V_y}{\partial \xi}+\dfrac{\partial V_y V_y}{\partial \eta}+\dfrac{\partial \eta}{\partial y}\dfrac{\partial p}{\partial \eta}=\dfrac{1}{\mathrm{Re}}\left(\left(\dfrac{\partial \xi}{\partial x}\right)^2\dfrac{\partial V_y}{\partial \xi^2}+\left(\dfrac{\partial \eta}{\partial y}\right)^2\dfrac{\partial^2 V_y}{\partial \eta^2}\right)-\dfrac{\partial \xi}{\partial x}\dfrac{\partial \vartheta_y \vartheta_x}{\partial \xi}-\dfrac{\partial \eta}{\partial y}\dfrac{\partial \vartheta_y \vartheta_y}{\partial \eta};\\
\dfrac{\partial \vartheta_x}{\partial t}+\dfrac{\partial \xi}{\partial x}\dfrac{\partial V_x \vartheta_x}{\partial \xi}+\dfrac{\partial \eta}{\partial y}\dfrac{\partial V_y \vartheta_x}{\partial \eta}=-\left(\vartheta_x\dfrac{\partial \xi}{\partial x}\dfrac{\partial V_x}{\partial \xi}+\vartheta_y\dfrac{\partial \eta}{\partial y}\dfrac{\partial V_x}{\partial \eta}\right)+C_s\left(-\left(\dfrac{\partial \xi}{\partial x}\dfrac{\partial V_y}{\partial \xi}-\dfrac{\partial \eta}{\partial y}\dfrac{\partial V_x}{\partial \eta}\right)\vartheta_y\right)+\\
\qquad+\dfrac{\partial \xi}{\partial x}\dfrac{\partial}{\partial \xi}\left(2\nu_{xx}\left(\dfrac{\partial \xi}{\partial x}\dfrac{\partial \vartheta_x}{\partial \xi}\right)\right)+\dfrac{\partial \eta}{\partial y}\dfrac{\partial}{\partial \eta}\left(\nu_{xy}\left(\dfrac{\partial \eta}{\partial y}\dfrac{\partial \vartheta_x}{\partial \eta}+\dfrac{\partial \xi}{\partial x}\dfrac{\partial \vartheta_y}{\partial \xi}\right)\right)-C_r\vartheta_x;\\
\dfrac{\partial \vartheta_y}{\partial t}+\dfrac{\partial \xi}{\partial x}\dfrac{\partial V_x \vartheta_y}{\partial \xi}+\dfrac{\partial \eta}{\partial y}\dfrac{\partial V_y \vartheta_y}{\partial \eta}=-\left(\vartheta_x\dfrac{\partial \xi}{\partial x}\dfrac{\partial \vartheta_y}{\partial \xi}+\vartheta_y\dfrac{\partial \eta}{\partial y}\dfrac{\partial V_y}{\partial \eta}\right)+C_s\left(\left(\dfrac{\partial \xi}{\partial x}\dfrac{\partial V_y}{\partial \xi}-\dfrac{\partial \eta}{\partial y}\dfrac{\partial V_x}{\partial \eta}\right)\vartheta_x\right)+\\
\qquad+\dfrac{\partial \xi}{\partial x}\dfrac{\partial}{\partial \xi}\left(\nu_{xy}\left(\dfrac{\partial \xi}{\partial x}\dfrac{\partial \vartheta_y}{\partial \xi}+\dfrac{\partial \eta}{\partial y}\dfrac{\partial \vartheta_x}{\partial \eta}\right)\right)+\dfrac{\partial}{\partial \eta}\left(2\nu_{yy}\dfrac{\partial \eta}{\partial y}\dfrac{\partial \vartheta_y}{\partial \eta}\right)-C_r\vartheta_y;\\
\dfrac{\partial \xi}{\partial x}\dfrac{\partial V_x}{\partial \xi}+\dfrac{\partial \eta}{\partial y}\dfrac{\partial V_y}{\partial \eta}=0.
\end{cases}
\tag{5}
$$

Here

$$
\nu_{xx}=\nu_{yy}=\frac{3}{\mathrm{Re}}+2\frac{S}{|\mathbf{defV}|},\ \nu_{xy}=\frac{3}{\mathrm{Re}}+2\left|\frac{\vartheta_x\vartheta_y}{\mathbf{defV}}\right|,\ S=\frac{\vartheta_x^2 J_x+\vartheta_y^2 J_y}{J_x+J_y},\ J_x=\left|\frac{\partial \xi}{\partial x}\frac{\partial \vartheta_x}{\partial \xi}\right|,\ J_y=\left|\frac{\partial \eta}{\partial y}\frac{\partial \vartheta_y}{\partial \eta}\right|,
$$

$$
|\mathbf{defV}|=\sqrt{2\left(\left(\frac{\partial \xi}{\partial x}\frac{\partial V_x}{\partial \xi}\right)^2+\left(\frac{\partial \eta}{\partial y}\frac{\partial V_y}{\partial \eta}\right)^2\right)+\left(\frac{\partial \xi}{\partial x}\frac{\partial V_y}{\partial \xi}+\frac{\partial \eta}{\partial y}\frac{\partial V_x}{\partial \eta}\right)^2}\ C_s=0.2,\ C_r=C_1\lambda_{\max}+C_2\frac{|\mathbf{d}\cdot\mathbf{v}|}{d^2}
$$

For numerical implementation, the system of equations (5) is reduced to a dimensionless form by correlating all velocities to the average velocity of the incoming flow. All linear dimensions are the length of the plates L.

Obvious boundary conditions of adhesion are set on all fixed solid walls: $V_x\big|_G=0$ and $V_y\big|_G=0$, where G is a solid boundary. At the channel output for horizontal, vertical velocities, and relative velocities, the conditions of extrapolation of the second order of accuracy are accepted. Uniform profiles of the longitudinal component of velocity with $V_x=U_0$ are applied at the inlet, and the transverse component of velocity and pressure is zero $V_y=P=0$. For the numerical implementation of the system (5), the following conditions were set at the input for relative velocities: $\vartheta_x=0.03$, $\vartheta_y=0$.

## 2 Solution method

The finite volume method is used for the numerical solution of the system of initial nonstationary equations (1). Due to the difficulties of matching the velocity and pressure fields, a grid with a spaced structure of the arrangement of grid nodes for dependent variables was used to discretize the equations of motion in directions and the continuity equation. This means that the velocity and pressure components are determined at different nodes. This approach is similar to the SIMPLE methods and gives certain advantages when

calculating the pressure field [13].

The fractional step method achieves the implicit connection of the terms pressure and velocity, which consists of two stages [14]. In the first stage, the intermediate velocities, $\bar{\Phi}_{i,j}^{n+\frac{1}{2}}$, are initially predicted without applying the incompressibility constraint using the two-stage explicit Runge-Kutta method as follows:

$$\begin{aligned}\bar{\Phi}_{i,j}^{n+\frac{1}{2}} &= \Phi_{i,j}^{n} + \frac{\Delta t}{2}\left[\Gamma^{n}\right],\\ \bar{\Phi}_{i,j}^{n+1} &= \Phi_{i,j}^{n} + \Delta t\left[\Gamma^{n+\frac{1}{2}}\right].\end{aligned} \tag{6}$$

Here

$$\Phi = \begin{pmatrix} V_x \\ V_y \\ \vartheta_x \\ \vartheta_y \end{pmatrix}, = \Gamma = \begin{pmatrix} -\frac{\partial V_x V_x}{\partial x} - \frac{\partial V_y V_x}{\partial y} + \frac{1}{\mathrm{Re}}\left(\frac{\partial^2 V_x}{\partial x^2} + \frac{\partial^2 V_x}{\partial y^2}\right) - \frac{\partial \vartheta_x \vartheta_y}{\partial y} - \frac{\partial \vartheta_x \vartheta_x}{\partial x} - \frac{\partial p^{n-\frac{1}{2}}}{\rho \partial x} \\ -\frac{\partial V_x V_y}{\partial x} - \frac{\partial V_y V_y}{\partial y} + \frac{1}{\mathrm{Re}}\left(\frac{\partial^2 V_y}{\partial x^2} + \frac{\partial^2 V_y}{\partial y^2}\right) - \frac{\partial \vartheta_y \vartheta_y}{\partial y} - \frac{\partial \vartheta_x \vartheta_y}{\partial x} - \frac{\partial p^{n-\frac{1}{2}}}{\rho \partial y} \\ -\frac{\partial V_x \vartheta_x}{\partial x} - \frac{\partial V_y \vartheta_x}{\partial y} - \left(\vartheta_x \frac{\partial V_x}{\partial x} + \vartheta_y \frac{\partial V_x}{\partial y}\right) + \frac{\partial}{\partial x}\left(2\nu_{xx}\frac{\partial \vartheta_x}{\partial x}\right) + \\ + \frac{\partial}{\partial y}\left(\nu_{xy}\left(\frac{\partial \vartheta_x}{\partial y} + \frac{\partial \vartheta_y}{\partial x}\right)\right) + C_s\left(-\left(\frac{\partial V_y}{\partial x} - \frac{\partial V_x}{\partial y}\right)\vartheta_y\right) - K_f \vartheta_x \\ -\frac{\partial V_x \vartheta_y}{\partial x} - \frac{\partial V_y \vartheta_y}{\partial y} - \left(\vartheta_x \frac{\partial V_y}{\partial x} + \vartheta_y \frac{\partial V_y}{\partial y}\right) + \frac{\partial}{\partial x}\left(\nu_{xy}\left(\frac{\partial \vartheta_y}{\partial x} + \frac{\partial \vartheta_x}{\partial y}\right)\right) + \\ + \frac{\partial}{\partial y}\left(2\nu_{yy}\frac{\partial \vartheta_y}{\partial y}\right) + C_s\left(\left(\frac{\partial V_y}{\partial x} - \frac{\partial V_x}{\partial y}\right)\vartheta_x\right) - K_f \vartheta_y \end{pmatrix}. \tag{7}$$

In the second stage, the intermediate velocities are projected onto vector fields without discrepancies using the Poisson equation, which calculates the increment of the pressure field, $\delta$p:

$$\nabla^2\left(\delta p\right) = \frac{1}{\Delta t}\left(\frac{\partial \bar{V}_x^{n+1}}{\partial x} + \frac{\partial \bar{V}_y^{n+1}}{\partial y}\right). \tag{8}$$

where $\nabla^2$ is the Laplace operator. Equation (8) is solved iteratively using the multigrid method [15], and the velocity field is updated as follows:

$$\begin{cases} V_x^{n+1} = \bar{V}_x^{n+1} - \Delta t \dfrac{\partial(\delta p)}{\partial x}, \\ V_y^{n+1} = \bar{V}_y^{n+1} - \Delta t \dfrac{\partial(\delta p)}{\partial y}. \end{cases} \tag{9}$$

$$p^{n+\frac{1}{2}} = p^{n-\frac{1}{2}} + \delta p. \tag{10}$$

Then the Poisson equation is solved using this new pressure, and an iterative process is established. The iteration continues until the condition that there are no discrepancies in the calculated velocity field within a certain tolerance is met.

The exact second-order approximations of the partial derivatives of the cell center in the continuity equation are read:

$$\left(\frac{\partial V_x}{\partial x}\right)_{i,j} = \frac{(V_x)_{i,j} - (V_x)_{i-1,j}}{\Delta x} + O(h^2), \left(\frac{\partial V_y}{\partial y}\right)_{i,j} = \frac{(V_y)_{i,j} - (V_y)_{i,j-1}}{\Delta y} + O(h^2). \tag{11}$$

Due to the staggered arrangement, the equations of x− and y-pulses are solved on the faces of the cells.

The exact discretization of the convective terms of the second order in the equation for longitudinal and transverse velocity is as follows:

$$\left(\frac{\partial V_x^2}{\partial x}\right)_{i,j} = \frac{\left((V_x)_{i+1,j} + (V_x)_{i,j}\right)^2 - \left((V_x)_{i,j} + (V_x)_{i-1,j}\right)^2}{4\Delta x} + O(h^2), \tag{12}$$

$$\left(\frac{\partial V_x V_y}{\partial y}\right)_{i,j} = \frac{\left((V_y)_{i+1,j} + (V_y)_{i,j}\right)\left((V_x)_{i,j+1} + (V_x)_{i,j}\right) - \left((V_y)_{i+1,j-1} + (V_y)_{i,j-1}\right)\left((V_x)_{i,j} + (V_x)_{i,j-1}\right)}{4\Delta y} + O(h^2),$$

$$\left(\frac{\partial V_x V_y}{\partial x}\right)_{i,j} = \frac{\left((V_x)_{i,j+1} + (V_x)_{i,j}\right)\left((V_y)_{i+1,j} + (V_y)_{i,j}\right) - \left((V_x)_{i-1,j+1} + (V_x)_{i-1,j}\right)\left((V_y)_{i,j} + (V_y)_{i-1,j}\right)}{4\Delta x} + O(h^2), \tag{13}$$

$$\left(\frac{\partial V_y^2}{\partial y}\right)_{i,j} = \frac{\left((V_y)_{i,j+1} + (V_y)_{i,j}\right)^2 - \left((V_y)_{i,j} + (V_y)_{i,j-1}\right)^2}{4\Delta y} + O(h^2),$$

a molar longitudinal and transverse velocity:

$$\begin{aligned} \left(\frac{\partial V_x \vartheta_x}{\partial x}\right)_{i,j} &= \frac{(V_x)_{i,j}\left((\vartheta_x)_{i+1,j} + (\vartheta_x)_{i,j}\right) - (V_x)_{i-1,j}\left((\vartheta_x)_{i,j} + (\vartheta_x)_{i-1,j}\right)}{2\Delta x} + O(h^2), \\ \left(\frac{\partial V_y \vartheta_x}{\partial y}\right)_{i,j} &= \frac{(V_y)_{i,j}\left((\vartheta_x)_{i,j+1} + (\vartheta_x)_{i,j}\right) - (V_y)_{i,j-1}\left((\vartheta_x)_{i,j} + (\vartheta_x)_{i,j-1}\right)}{2\Delta x} + O(h^2), \end{aligned} \tag{14}$$

$$\left(\frac{\partial V_x \vartheta_y}{\partial x}\right)_{i,j} = \frac{(V_x)_{i,j}\left((\vartheta_y)_{i+1,j} + (\vartheta_y)_{i,j}\right) - (V_x)_{i-1,j}\left((\vartheta_y)_{i,j} + (\vartheta_y)_{i-1,j}\right)}{2\Delta x} + O\left(h^2\right),$$
$$\left(\frac{\partial V_y \vartheta_y}{\partial y}\right)_{i,j} = \frac{(V_y)_{i,j}\left((\vartheta_y)_{i,j+1} + (\vartheta_y)_{i,j}\right) - (V_y)_{i,j-1}\left((\vartheta_y)_{i,j} + (\vartheta_y)_{i,j-1}\right)}{2\Delta x} + O\left(h^2\right), \quad (15)$$

The exact discretization of the second-order diffusion terms in the equation for all velocities are as follows:

$$\left(\frac{\partial^2 \Phi}{\partial x^2}\right)_{i,j} = \frac{(\Phi)_{i+1,j} - 2(\Phi)_{i,j} + (\Phi)_{i-1,j}}{(\Delta x)^2} + O\left(h^2\right),$$
$$\left(\frac{\partial^2 \Phi}{\partial y^2}\right)_{i,j} = \frac{(\Phi)_{i,j+1} - 2(\Phi)_{i,j} + (\Phi)_{i,j-1}}{(\Delta y)^2} + O\left(h^2\right). \quad (16)$$
$$\Phi = V_x, V_y.$$

$$\left(\frac{\partial}{\partial x}\left(\mathrm{A}\frac{\partial \Phi}{\partial x}\right)\right)_{i,j} = \frac{\left(\mathrm{A}_{i,j} + \mathrm{A}_{i+1,j}\right)}{2\Delta x^2}\Phi_{i+1,j} - \frac{\left(\mathrm{A}_{i-1,j} + 2\mathrm{A}_{i,j} + \mathrm{A}_{i+1,j}\right)}{2\Delta x^2}\Phi_{i,j} + \frac{\left(\mathrm{A}_{i,j} + \mathrm{A}_{i-1,j}\right)}{2\Delta x^2}\Phi_{i-1,j} + O\left(h^2\right),$$
$$\left(\frac{\partial}{\partial y}\left(\mathrm{A}\frac{\partial \Phi}{\partial y}\right)\right)_{i,j} = \left(\frac{\left(\mathrm{A}_{i,j} + \mathrm{A}_{i,j+1}\right)}{2\Delta y^2}\Phi_{i,j+1} - \frac{\left(\mathrm{A}_{i,j-1} + 2\mathrm{A}_{i,j} + \mathrm{A}_{i,j+1}\right)}{2\Delta y^2}\Phi_{i,j} + \frac{\left(\mathrm{A}_{i,j} + \mathrm{A}_{i,j-1}\right)}{2\Delta y^2}\Phi_{i,j-1}\right) + O\left(h^2\right),$$
$$\left(\frac{\partial}{\partial x}\left(\mathrm{A}\frac{\partial \Phi}{\partial y}\right)\right)_{i,j} = \frac{1}{2\Delta x}\left(\mathrm{A}_{i,j+1}\left(\frac{\Phi_{i+1,j+1} - \Phi_{i+1,j-1}}{2\Delta y}\right) - \mathrm{A}_{i,j-1}\left(\frac{\Phi_{i-1,j+1} - \Phi_{i-1,j-1}}{2\Delta y}\right)\right) + O\left(h^2\right),$$
$$\Phi = \vartheta_x, \vartheta_y, \quad \mathrm{A} = v_{xy}, v_{xx}, v_{yy}.$$

And for the Poisson equation, it is estimated as:

$$\left(\frac{\partial^2 \delta p}{\partial x^2}\right)_{i,j} = \frac{(\delta p)_{i+1,j} - 2(\delta p)_{i,j} + (\delta p)_{i-1,j}}{(\Delta x)^2} + O\left(h^2\right),$$
$$\left(\frac{\partial^2 \delta p}{\partial y^2}\right)_{i,j} = \frac{(\delta p)_{i,j+1} - 2(\delta p)_{i,j} + (\delta p)_{i,j-1}}{(\Delta y)^2} + O\left(h^2\right). \quad (17)$$

Exact approximations of the fourth order of partial derivatives along the center of the cell in the continuity equation:

$$\left(\frac{\partial V_x}{\partial x}\right)_{i,j} = \frac{-(V_x)_{i+1,j} + 27(V_x)_{i,j} - 27(V_x)_{i-1,j} + (V_x)_{i-2,j}}{24\Delta x} + O\left(h^4\right),$$
$$\left(\frac{\partial V_y}{\partial y}\right)_{i,j} = \frac{-(V_y)_{i,j+1} + 27(V_y)_{i,j} - 27(V_y)_{i,j-1} + (V_y)_{i,j-2}}{24\Delta y} + O\left(h^4\right), \quad (18)$$

The exact discretization of the convective terms of the fourth order in the equation for longitudinal and transverse velocity is as follows:

$$\left(\frac{\partial V_x^2}{\partial x}\right)_{i,j} = \frac{-\left(\tilde{V}_x\right)_{i+2,j}^2 + 27\left(\tilde{V}_x\right)_{i+1,j}^2 - 27\left(\tilde{V}_x\right)_{i,j}^2 + \left(\tilde{V}_x\right)_{i-1,j}^2}{24\Delta x} + O\left(h^4\right),$$
$$\left(\frac{\partial V_x V_y}{\partial y}\right)_{i,j} = \frac{-\left(\tilde{V}_x\right)_{i,j+1}^C \left(\tilde{V}_y\right)_{i,j+1}^C + 27\left(\tilde{V}_x\right)_{i,j}^C \left(\tilde{V}_y\right)_{i,j}^C - 27\left(\tilde{V}_x\right)_{i,j-1}^C \left(\tilde{V}_y\right)_{i,j-1}^C + \left(\tilde{V}_x\right)_{i,j-2}^C \left(\tilde{V}_y\right)_{i,j-2}^C}{24\Delta y} + O\left(h^4\right), \quad (19)$$

$$\left(\frac{\partial V_x V_y}{\partial x}\right)_{i,j} = \frac{-\left(\tilde{V}_x\right)_{i+1,j}^C \left(\tilde{V}_y\right)_{i+1,j}^C + 27\left(\tilde{V}_x\right)_{i,j}^C \left(\tilde{V}_y\right)_{i,j}^C - 27\left(\tilde{V}_x\right)_{i-1,j}^C \left(\tilde{V}_y\right)_{i-1,j}^C + \left(\tilde{V}_x\right)_{i-2,j}^C \left(\tilde{V}_y\right)_{i-2,j}^C}{24\Delta x} + O\left(h^4\right),$$
$$\left(\frac{\partial V_y^2}{\partial y}\right)_{i,j} = \frac{-\left(\tilde{V}_y\right)_{i,j+2}^2 + 27\left(\tilde{V}_y\right)_{i,j+1}^2 - 27\left(\tilde{V}_y\right)_{i,j}^2 + \left(\tilde{V}_y\right)_{i,j-1}^2}{24\Delta x} + O\left(h^4\right). \quad (20)$$

a molar longitudinal and transverse velocity:

$$\left(\frac{\partial V_x \vartheta_x}{\partial x}\right)_{i,j} = \frac{-\left(\tilde{V}_x\right)_{i+1,j}^C \left(\tilde{\vartheta}_x\right)_{i+1,j}^C + 27\left(\tilde{V}_x\right)_{i,j}^C \left(\tilde{\vartheta}_x\right)_{i,j}^C - 27\left(\tilde{V}_x\right)_{i-1,j}^C \left(\tilde{\vartheta}_x\right)_{i-1,j}^C + \left(\tilde{V}_x\right)_{i-2,j}^C \left(\tilde{\vartheta}_x\right)_{i-2,j}^C}{24\Delta x} + O\left(h^4\right),$$
$$\left(\frac{\partial V_y \vartheta_x}{\partial y}\right)_{i,j} = \frac{-\left(\tilde{V}_y\right)_{i,j+1}^C \left(\tilde{\vartheta}_x\right)_{i,j+1}^C + 27\left(\tilde{V}_y\right)_{i,j}^C \left(\tilde{\vartheta}_x\right)_{i,j}^C - 27\left(\tilde{V}_y\right)_{i,j-1}^C \left(\tilde{\vartheta}_x\right)_{i,j-1}^C + \left(\tilde{V}_y\right)_{i,j-2}^C \left(\tilde{\vartheta}_x\right)_{i,j-2}^C}{24\Delta y} + O\left(h^4\right). \quad (21)$$

$$\left(\frac{\partial V_x \vartheta_y}{\partial x}\right)_{i,j} = \frac{-\left(\tilde{V}_x\right)_{i+1,j}^C \left(\tilde{\vartheta}_y\right)_{i+1,j}^C + 27\left(\tilde{V}_x\right)_{i,j}^C \left(\tilde{\vartheta}_y\right)_{i,j}^C - 27\left(\tilde{V}_x\right)_{i-1,j}^C \left(\tilde{\vartheta}_y\right)_{i-1,j}^C + \left(\tilde{V}_x\right)_{i-2,j}^C \left(\tilde{\vartheta}_y\right)_{i-2,j}^C}{24\Delta x} + O\left(h^4\right),$$
$$\left(\frac{\partial V_y \vartheta_y}{\partial y}\right)_{i,j} = \frac{-\left(\tilde{V}_y\right)_{i,j+1}^C \left(\tilde{\vartheta}_y\right)_{i,j+1}^C + 27\left(\tilde{V}_y\right)_{i,j}^C \left(\tilde{\vartheta}_y\right)_{i,j}^C - 27\left(\tilde{V}_y\right)_{i,j-1}^C \left(\tilde{\vartheta}_y\right)_{i,j-1}^C + \left(\tilde{V}_y\right)_{i,j-2}^C \left(\tilde{\vartheta}_y\right)_{i,j-2}^C}{24\Delta y} + O\left(h^4\right). \quad (22)$$

The exact discretization of the fourth-order diffusion terms in the equation for all velocities are as follows:

$$\left(\frac{\partial^2 \Phi}{\partial x^2}\right)_{i,j} = \frac{-\left(\Phi\right)_{i+2,j} + 16\left(\Phi\right)_{i+1,j} - 30\left(\Phi\right)_{i,j} + 16\left(\Phi\right)_{i-1,j} - \left(\Phi\right)_{i-2,j}}{12\left(\Delta x\right)^2} + O\left(h^4\right),$$
$$\left(\frac{\partial^2 \Phi}{\partial y^2}\right)_{i,j} = \frac{-\left(\Phi\right)_{i,j+2} + 16\left(\Phi\right)_{i,j+1} - 30\left(\Phi\right)_{i,j} + 16\left(\Phi\right)_{i,j-1} - \left(\Phi\right)_{i,j-2}}{12\left(\Delta y\right)^2} + O\left(h^4\right). \quad (23)$$
$$\Phi = V_x, V_y.$$

Where $\left(\tilde{V}_x\right)_{i,j}$ and $\left(\tilde{V}_y\right)_{i,j}$ are the interpolated velocities:

$$\left(\tilde{V}_x\right)_{i,j} = \frac{-\left(V_x\right)_{i+1,j} + 9\left(V_x\right)_{i,j} + 9\left(V_x\right)_{i-1,j} - \left(V_x\right)_{i-2,j}}{16} + O\left(h^4\right),$$
$$\left(\tilde{V}_y\right)_{i,j} = \frac{-\left(V_y\right)_{i,j+1} + 9\left(V_y\right)_{i,j} + 9\left(V_y\right)_{i,j-1} - \left(V_y\right)_{i,j-2}}{16} + O\left(h^4\right). \quad (24)$$

and $\left(\tilde{V}_x\right)_{i,j}^C$, $\left(\tilde{V}_y\right)_{i,j}^C$, $\left(\tilde{\vartheta}_x\right)_{i,j}^C$, $\left(\tilde{\vartheta}_y\right)_{i,j}^C$ are the interpolated velocities:

$$\begin{aligned}
\left(\tilde{V}_x\right)_{i,j}^C &= \frac{-\left(V_x\right)_{i,j+2}+9\left(V_x\right)_{i,j+1}+9\left(V_x\right)_{i,j}-\left(V_x\right)_{i,j-1}}{16}+O\left(h^4\right),\\
\left(\tilde{V}_y\right)_{i,j}^C &= \frac{-\left(V_y\right)_{i+2,j}+9\left(V_y\right)_{i+1,j}+9\left(V_y\right)_{i,j}-\left(V_y\right)_{i-1,j}}{16}+O\left(h^4\right),\\
\left(\tilde{\vartheta}_x\right)_{i,j}^C &= \frac{-\left(\vartheta_x\right)_{i,j+2}+9\left(\vartheta_x\right)_{i,j+1}+9\left(\vartheta_x\right)_{i,j}-\left(\vartheta_x\right)_{i,j-1}}{16}+O\left(h^4\right),\\
\left(\tilde{\vartheta}_y\right)_{i,j}^C &= \frac{-\left(\vartheta_y\right)_{i+2,j}+9\left(\vartheta_y\right)_{i+1,j}+9\left(\vartheta_y\right)_{i,j}-\left(\vartheta_y\right)_{i-1,j}}{16}+O\left(h^4\right).
\end{aligned} \tag{25}$$

**Table 1**. Two types of a sample of a finite difference scheme and their order of accuracy.

| Of course, the difference scheme and their order of accuracy | $\left(\frac{\partial V_x\Phi}{\partial x}\right)$, $\left(\frac{\partial V_y\Phi}{\partial y}\right)$ $\Phi = V_x, V_y, \vartheta_x, \vartheta_y.$ | $\left(\frac{\partial^2\Phi}{\partial x^2}\right)$, $\left(\frac{\partial^2\Phi}{\partial y^2}\right)$ $\Phi = V_x, V_y, \vartheta_x, \vartheta_y, \delta p.$ | $\left(\frac{\partial^2\delta p}{\partial x^2}\right)$, $\left(\frac{\partial^2\delta p}{\partial y^2}\right)$. | $\left(\frac{\partial}{\partial x}\mathrm{A}\left(\frac{\partial\Phi}{\partial x}\right)\right)$, $\left(\frac{\partial}{\partial y}\mathrm{A}\left(\frac{\partial\Phi}{\partial y}\right)\right)$ $\Phi = \vartheta_x, \vartheta_y.$ $\mathrm{A} = \nu_{xy}, \nu_{xx}, \nu_{yy}.$ | $\left(\frac{\partial V_x}{\partial x}\right), \left(\frac{\partial V_y}{\partial y}\right)$ |
|---|---|---|---|---|---|
| Scheme A | 2 | 2 | 2 | 2 | 2 |
| Scheme B | 4 | 4 | 2 | 2 | 4 |

The integration was carried out in time steps for Scheme A-Δt=0.001 and for Scheme B-Δt=0.0001.

## 3 Results and Discussion

The comparisons of the numerical results obtained with the known experimental data are shown below. 3 shows the numerical results of changing the Reynolds number of the momentum loss's thickness from the plate's dimensionless length. The Reynolds number of the momentum loss thickness was found by integrating the equation

$$\frac{d\,\mathrm{Re}_\theta}{dx} = 0.5C_f. \tag{26}$$

Here $C_f$ is plate friction coefficient:

$$C_f = \frac{2}{\mathrm{Re}}\left(\frac{\partial V_x}{\partial y}\right). \tag{27}$$

Figure 3 shows experimental results for the comparison of rhombuses

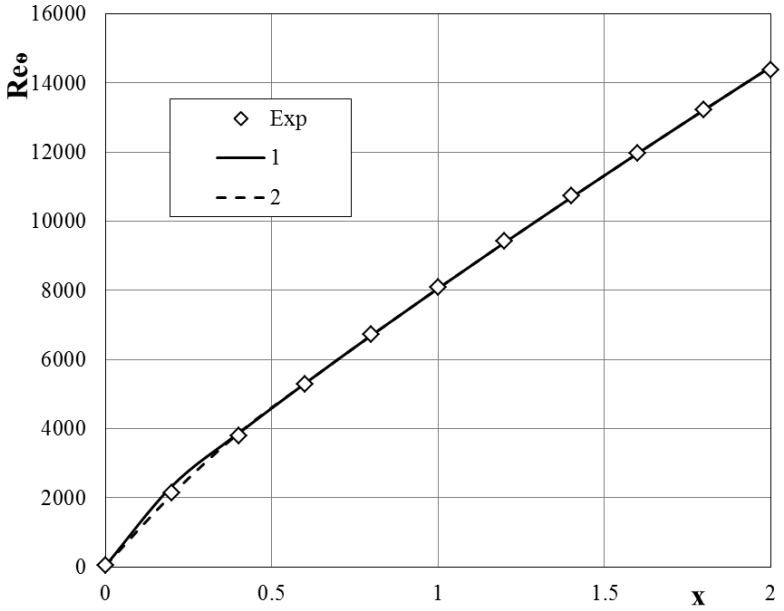


**Fig. 3.** The dependence of the Reynolds number of the pulse loss thickness on the length of the plate: 1 is results of scheme A, 2 is results of scheme B.

Figure 4 shows a solid line showing the dependence of the coefficient of friction on the dimensionless thickness of the momentum loss according to the proposed model. Lozenges is also illustrated by the results of the Karman-Schoenherr theory [16].

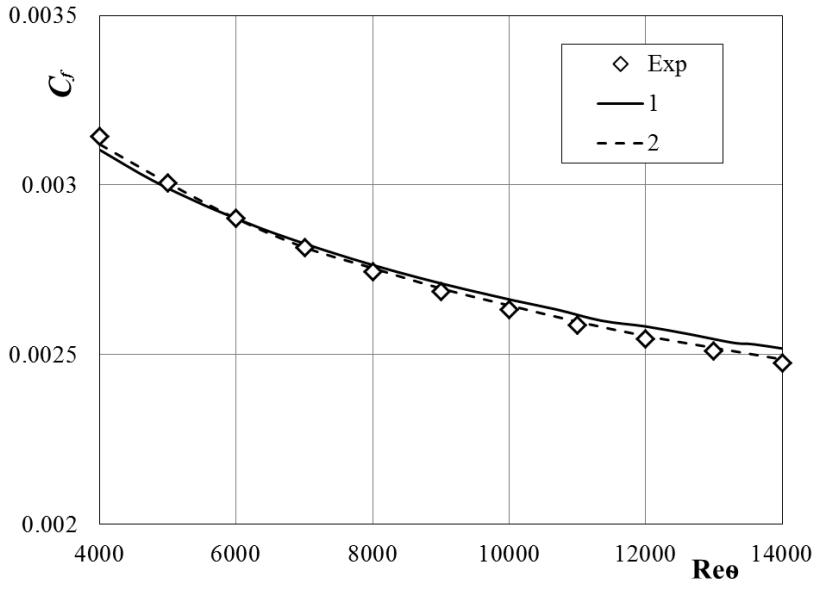


**Fig.4.** The dependence of the coefficient of friction on the Reynolds number of the thickness of the momentum loss: 1 is results of scheme A, 2 is the results of scheme B.

In figure 5, a solid line shows the result of numerical calculation for a dimensionless longitudinal flow velocity depending on the dimensionless distance to the plate. The formulas determined dimensionless speeds and distances

$$u^+ = \frac{V_x}{u^*}, \quad y^+ = \mathrm{Re}\, y u^*, \; u^* = \sqrt{0.5 C_f}. \tag{28}$$

Here, for comparison with the results of the rhombic model, the results of the Coles theory are also shown [17, 18].

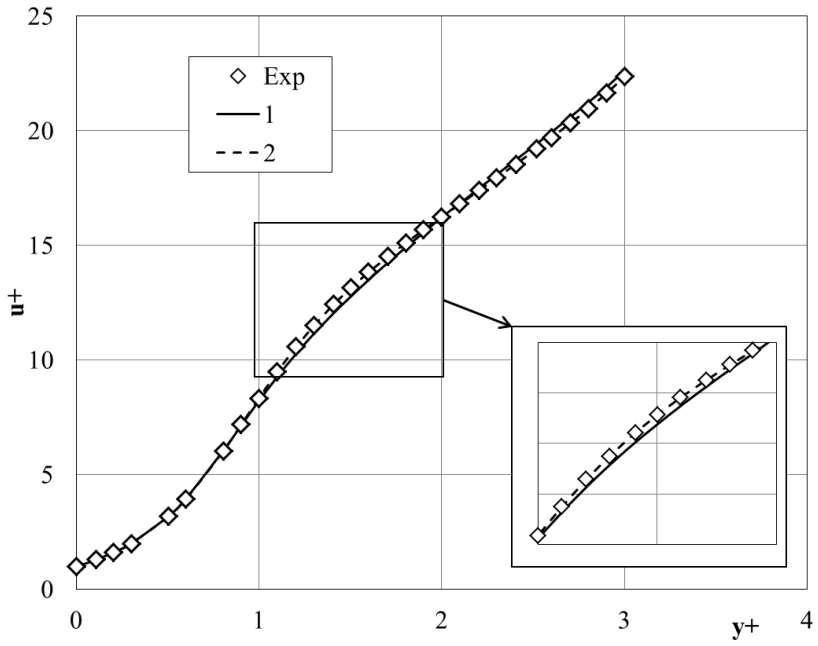


**Fig. 5.** The transverse distribution of the longitudinal velocity: 1 is results of scheme A, 2 is results of scheme B.

## 4 Conclusion

The paper presents numerical solutions for the flow of an incompressible viscous fluid into the flow around a flat plate using a new two-fluid turbulent model. The dependence of the Reynolds number on the thickness of the momentum loss, the dependence of the coefficient of friction on the Reynolds number of the thickness of the momentum loss, and the transverse distribution of the longitudinal velocity are demonstrated. For the numerical implementation of the turbulence equation, second- and fourth-order accuracy schemes are used. From the figure, it can be seen both schemes satisfy the experimental results. But when using methods of the fourth order of accuracy, an increase in the algorithm's accuracy has to be paid for by increasing the calculation time and complicating the difference scheme. This should be carefully considered when choosing a method for solving partial differential equations. Usually, for most problems of hydrodynamics, sufficient accuracy can be obtained by methods of the second order of accuracy.

## References

1. Boussinesk J., Essai sur la théorie des eaux courantes.-Paris: Mémoires présentées par diverses savants à l'Acad. D. Sci., **23,** (1877)
2. Prandtl L. Untersuchungen zur ausgebildeteTurbulenz.-Zeitschr. f. Angew. Math. u. Mech., **5**, (1925)
3. Karman Th. Mechanische Ahnlichkeit und Turbulenz. – Nachr. d. Gesellsch. d. Wissen. Zu Gottingen, Math. Phys. Kl., (1930)
4. Spalart P. R., Allmaras S. R. Aone-equation turbulence model for aerodynamic flows. AIAA p.0439, (1992)
5. Menter F. R."Zonal two-equation k-ω turbulence models for aerodynamic flows". AIAAPaper 1993-2906.
6. Menter F. R., Kuntz M., and Langtry R. "TenYears of Industrial Experience with the SST Turbulence Model". Turbulence, Heat and Mass Transfer 4, ed: K. Hanjalic, Y. Nagano, and M. Tummers, Begell House, pp. 625 - 632 (2003)
7. Erkinjon son M.M. Numerical Calculation of an Air Centrifugal Separator Based on the SARC Turbulence Model, J. Appl. Comput. Mech., **7**(2), (2021) https://doi.org/10.22055/JACM.2020.31423.1871
8. Malikov Z.M., Madaliev M.E. Numerical Simulation of Two-Phase Flow in a Centrifugal Separator. Fluid Dynamics. **55**(8). pp. 1012–1028 (2020) doi: 10.1134/S0015462820080066
9. Malikov Z. "Mathematical Model of Turbulence Based on the Dynamics of Two Fluids". Applied Mathematical Modeling. **82,** pp. 409-436 (2020)
10. Cristopher R Responsible NASA official. Turbulence modeling Resource. NASA Langley Research Center, http://turbmodels.larc.nasa.gov. (accessed date 04.04.2019)
11. Malikov Z.M., Madaliev M.E. New two-fluid turbulence model-based numerical simulation of flow in a flat suddenly expanding channel. Herald of the Bauman Moscow State Technical University, Series Natural Sciences, **4**(97), pp. 24–39 (2021) https://doi.org/10.18698/1812-3368-2021-4-24-39
12. Anderson D, Tannehill J, Pletcher R. Computational fluid mechanics and heat transfer. -M.: Mir, **1**, (1990)
13. Patankar S.V. Numerical Heat Transfer and Fluid Flow. Taylor&Francis. (1980)
14. Cevheri M., McSherry R., and Stoesser T. A local mesh refinement approach for large-eddy simulations of turbulent flows. International Journal for Numerical Methods in Fluids, **82**(5), 261-285 (2016)
15. A. A. Mirzoev, M. Madaliev, and D. Y. Sultanbayevich. Numerical modeling of nonstationary turbulent flow with double barrier based on two liquid turbulence model. in 2020 International Conference on Information Science and Communications Technologies (ICISCT). 1–7. (2020)
16. Schoenherr K. E. Resistance of flat plate. Trans. SNAME. **40**, pp. 279-313, (1932)
17. Coles D. E. The law of the wake in the turbulent boundary layer. J. Fluid Mech. **1**, pp.191–226, (1956)
18. Coles D. The turbulent boundary layer in a compressible fluid. J. Fluid Mech. **1**, p.191. Rep.R-403-PR, Rand Corp., Santa Monica, California (1962)